Integration of Motor Unit Filters for Enhanced Surface Electromyogram Decomposition During Varying Force Isometric Contraction

Miaojuan Xia, Chen Chen, *Member, IEEE*, Xinjun Sheng, *Member, IEEE*, and Han Ding

Abstract—**Muscles generate varying levels of force by recruiting different numbers of motor units (MUs), and as the force increases, the number of recruited MUs gradually rises. However, current decoding methods encounter difficulties in maintaining a stable and consistent growth trend in MU numbers with increasing force. In some instances, an unexpected reduction in the number of MUs can even be observed as force intensifies. To address this issue, in this study, we propose an enhanced decoding method that adaptively reutilizes MU filters. Specifically, in addition to the normal decoding process, we introduced an additional procedure where MU filters are reused to initialize the algorithm. The MU filters are iterated and adapted to the new signals, aiming to decode motor units that were actually activated but cannot be identified due to heavy superimposition. We tested our method on both simulated and experimental surface electromyogram (sEMG) signals. We simulated isometric signals (10%-70%) with known MU firing patterns using experimentally recorded MU action potentials from forearm muscles and compared the decomposition results to two baseline approaches: convolution kernel compensation (CKC) and fast independent component analysis (fastICA). Our method increased the decoded MU number by a rate of 135.4% ± 62.5% and 63.6% ± 20.2% for CKC and fastICA, respectively, across different signal-to-noise ratios. The sensitivity and precision for MUs decomposed using the enhanced method remained at the same accuracy level (p < 0.001) as those of normally decoded MUs. For the experimental signals, eight healthy subjects performed hand movements at five different force levels (10%-90%), during which sEMG signals were recorded and decomposed. The results indicate that the enhanced process increased the number of decoded MUs by 21.8% ± 10.9% across all subjects. We discussed the possibility of fully capturing all activated motor units by appropriately reusing previously decoded MU filters and**

improving the balance of activated motor unit numbers across varying excitation levels.

Index Terms—**Motor unit (MU), firing pattern, decomposition, high-density electromyogram, action potential, excitation level.**

I. Introduction

OVER the past decades, there's been a surge in methodologies for extracting individual motor unit activities from sEMG signals. This noninvasive approach provides valuable insights into synaptic input through motor unit discharge timings [1]. Proposed methods include template-matching [2], mathematical modeling (PCA: Principal Component Analysis, ICA: Independent Component Analysis, NMF: Non-negative Matrix Factorization) [3], [4], [5], [6], and convolutive blind source separation (BSS) [7], [8]. Deep learning approaches have also been introduced to uncover hidden relations within high-dimensional sEMG signals, especially in the era of big data [9], [10], [11], [12]. Although various decomposition algorithms have been proposed, it is observed that the number of motor units did not exhibit the expected increase along ascending force levels, contrary to the predictions of the size principle [13]. Occasionally, higher force resulted in fewer decomposed motor units [14]. The decomposition algorithm encounters challenges when simultaneously decomposing both larger and smaller motor units, particularly in scenarios with high excitation levels and substantial recruitment of motor units. This difficulty can be attributed to the significant size difference among motor units, where the number of fibers in larger motor units is dozens or even hundreds of times greater than that in smaller ones [15]. Consequently, the amplitude of motor unit action potentials exhibits substantial variability. When larger motor units are activated, the signals produced by smaller motor units become minimal due to heavy superimposition and may be mistakenly classified as noise.

There has been considerable research on the reuse of MU filters. Some studies have applied MU filters directly to new signals [16], but this approach carries the risk of reduced decoding accuracy. To address the complexity of sEMG signals, some dynamic and real-time decoding studies have employed active updates to MU filters [5], [17]. Specifically, MU filters are derived from the initial filter and updated by

subsequent small signal intervals to form the final decoding filter. This method intentionally considers every incremental change, making its long-term stability challenging to guarantee. However, once the final MU filter is formed, it still lacks a final adaptation process for accurately locating and decoding the discharges of the motor unit represented by the MU filter. We believe that it is not always necessary to update the MU filter, and even if updates are made, it is difficult to ensure that the update direction is correct. Instead, we need to appropriately guide the algorithm to converge in a specific direction.

The force exerted by a muscle during a voluntary contraction depends on the recruitment of motor units and rate coding. In the neural control field, the cumulative spike train (CST) is commonly used to estimate force, representing the sum of all motor unit firings and directly correlating with muscle force [18], [19], [20]. The increase in the discharge rate of CST is commonly attributed to two factors: the introduction of new motor units and an inherent rise in the discharge frequency of pre-existing motor units [21]. However, the decoding-related loss of smaller motor units can lead to an insignificant or even reduced increase of CST, particularly during higher force exertion. This introduces notable errors in force estimation based on CST. While a strong correlation between CST and force may exist under normal conditions, abrupt increases in applied force can result in significant deviations in the CST trend [22], [23].

Our study introduces an enhanced strategy to address discrepancies in motor unit decomposition across varying force levels. By adaptively integrating prelearned motor unit filters from lower force levels into higher force analyses, our approach demonstrates the ability to uncover more reliable motor units at higher force levels. We validated our proposal using both simulated and experimental signals. The results showed a substantial increase in the number of decoded motor units across varying SNRs and subjects. This research advances our understanding of neuromuscular control and enhances the accuracy of force estimation through cumulative spike train analysis.

II. METHOD

A. Algorithm

The generation model of multi-channel sEMG signals can be described as a convolutive mixture of a series of impulses, representing the discharge pattern of motor units [24]:

$$y_i(n) = \sum_{j=1}^{J} \sum_{l=0}^{L-1} h_{ij}(l) s_j(n-l) + w_i(n) \tag{1}$$

where $y_i(n)$ is the ith sEMG channel, n is the discrete sample point, $w_i(n)$ is the additive noise at channel i, $h_{ij}(l)$ is the action potential of the jth motor unit recorded at channel i, L is the sample length of the action potential, $s_j(n)$ is the spike train of the jth motor unit, J is the number of active motor units. The CKC method compensates for the unknown mixing kernel h_{ij} and estimates the spike train of the jth motor unit using a linear minimum mean square error estimator as [25]:

$$\hat{s}_j(n) = c_{s_j \bar{y}}^T C_{\bar{y}\bar{y}}^{-1} \bar{y}(n) \tag{2}$$

where $C_{\bar{y}\bar{y}} = E(\bar{y}(n)\bar{y}^T(n))$ is the correlation matrix of measurements, $\bar{y}$ is the extended sEMG signals by adding K delayed versions, K is the extending length and was set as 10 in this work. $c_{s_j \bar{y}} = E(y(n)s_j^T(n))$ is cross-correlation vector, and $E(.)$ denotes mathematical expectation. The estimation of the jth IPT in (2) requires the cross-correlation vector $c_{s_j \bar{y}}$ to be known in advance. In the first iteration step, this unknown cross-correlation vector $c_{s_j \bar{y}}$ is blindly chosen and approximated by vector of measurements $\hat{c}_{s_j \bar{y}} = y(n_1)$ where the time instance n_1 is assumed to discharge from the jth motor unit. Specifically, the time instance n_1 is determined by the so called activity index [24]:

$$\gamma(n) = \bar{y}^T C_{\bar{y}\bar{y}}^{-1} \bar{y}(n) \tag{3}$$

where the activity index $\gamma = \{\gamma(n); n = 0, 1, \ldots\}$ can be thought of as an indicator of global pulse train activity, i.e., $\gamma(n_k) > 0 \Leftrightarrow \exists j : \bar{s}_j(n_k) = 1$. Similarly in the fastICA algorithm [3], the time instant n_1 was located to the maximum of the squared summation of all whitened extended observation and $c_{s_j \bar{y}}$ was initialized at the same time instant. The whitening process can accelerate the algorithm but it can not distinguish the strength of the components. Consequently, in cases where the amplitude of different motor units varies significantly—by dozens to hundreds of times—the activity index becomes severely biased towards larger motor units, treating the activities from smaller motor units as physiological noise. Although the activity index has proven efficient for lower force signals, it becomes flawed at higher force levels where sEMG signals are dominated by relatively large motor unit action potentials (MUAPs). Proper initialization ensures that each iteration of the loop contributes effectively towards achieving the desired result.

In this study, we proposed an alternative initialization method using the MU Filters decomposed from lower force signals. According to the size principle and previous studies [16], MU filters transferred from low to high contraction levels has been proven to be efficient. Consequently, only the MU filters from lower contraction levels were used. The right column represents the normal decomposition process for new signals (Figure 1). We used two different basic decoding algorithms (CKC [24] and fastICA [3]) in our study, but the process is not limited to these methods. The left column illustrates the proposed enhanced decomposition process. In this approach, MU filters $c_{s_j \bar{y}}$ acquired from lower force levels were used as initialization vectors. For example, when decomposing signals at the 70% force level, MU filters from the 10%, 30%, and 50% force levels were collected and utilized in this process. After two iterative steps, we obtained the pulses converged from the MU filters. Specifically, we applied fixed-point iteration (same as fastICA) in the first iteration. Following this, the spike train was estimated using Equation 2, and the MU filter $c_{s_j \bar{y}}$ was updated by $c_{s_j \bar{y}} = E(y(n)s_j^T(n))$. This second iterative process, derived from CKC, was repeated k times until we achieved the final result. In this study, k was set to 5. To avoid duplication, only pulses with a Rate of Agreement (RoA) lower than 0.3 were accepted as new pulses. Compared to direct reuse, our method includes two iterative processes initiated from the MU filter. These iterations allow the MU
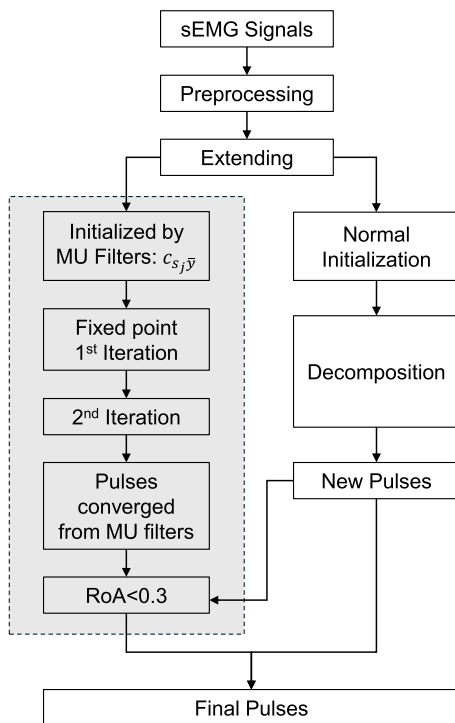
Fig. 1. Flowchart diagram of signal processing: The signals were first decoded by the normal decomposition process (right column) and then applied in an enhanced decomposition process (left column). Only pulses with RoA < 0.3 (compared to normally decoded pulses) were kept.

filters to adapt to new signals, addressing inevitable changes due to superimposition at higher levels and acquiring more accurate results.

B. Simulated Signal

Simulated sEMG signals were created by convolving synthetic motor unit spike trains (MUSTs) with experimentally obtained motor unit action potentials. MUAPs were extracted from previous experimental sEMG signals using high-density electrode arrays [19]. All the MUAPs were experimentally acquired from twelve subjects in the forearm muscles. Each motor pool consisted of one hundred motor units, distributed according to the size principle in [26], with recruitment thresholds following an exponential function in size order. Units with fewer muscle fibers were recruited first, initially firing at 8 Hz up to a maximum of 35 Hz [27]. Seven different muscle excitation levels were simulated: 10%, 20%, 30%, 40%, 50%, 60%, and 70%, resulting in 52, 73, 84, 93, 100, 100, and 100 active MUs, respectively. For each excitation level, four signal-to-noise ratios (SNR: 20dB, 25dB, 30dB, ∞dB) were simulated. A total of 168 (7 Excitation levels × 4 SNRs × 6 MU pools) simulations were conducted using six different motor pools.

We also conducted a second simulation to illustrate the difference in size and depth of motor units decomposed using normal and enhanced decomposition methods in Figure 8. In this simulation, 100 motor units were modeled based on an anatomical framework consisting of a cylindrical volume conductor with an anisotropic muscle layer, and isotropic bone,

subcutaneous, and skin layers [28]. The simulated muscle tissue comprised over 4,000 fibers with an average diameter of 56 μm, with each motor unit consisting of 15 to 1,500 fibers. The motor units had a normally distributed conduction velocity of 4.0 ± 0.35 m/s, with the slowest velocity assigned to the smallest motor unit, ranging from 3.01 m/s to 4.94 m/s. The detection system used a grid of 11 × 17 circular electrodes (diameter 1 mm) with an inter-electrode distance of 5 mm. Motor units within the motor pool are distributed according to the size principle [26]. The recruitment thresholds, activated number, and firing frequency were determined by the rate coding model in [27], consistent with the first simulation.

C. Experimental Signal

1) Participants: Eight healthy subjects (8 males; age: 27 ± 5 yrs; height:170 ± 12cm) participated in this experiment. The subjects did not have any history of neuromuscular disorders and gave written informed consent before participating in this study. The experiment protocol was in accordance with the Declaration of Helsinki and approved by the local ethic committee (approved number B2020026I).

2) Experimental Protocol: The experimental session involved a series of grasping tasks targeting the hands, designed to fully activate the motor pool across a broad force range. Conducted on the dominant forearm, the experiment measured the myoelectrical activity of forearm muscles using high-density sEMG. Participants were seated in front of a computer screen, with their dominant forearm grasping an S-shaped transducer (CCT transducers model TF 022, range 100 kg, sampling rate 10,000 Hz). During the familiarization phase, each task was carefully explained to the subjects. Before the experiment, their maximum voluntary contraction (MVC) was measured for 3 repetitions. Subsequently, the participant performed isometric contractions (make a fist) at five different force levels (10%, 30%, 50%, 70%, 90%), each level repeated four trials. The task required control of a cursor to trace a trapezoidal force curve displayed on the screen. Each session included a 1-second ramp-up to the targeted force level, followed by an 8-second flat phase, and a 1-second ramp-down. Each trial lasts 10 seconds and a 5-second rest interval. During the experiment, participants were often asked if there was any fatigue, in such cases 30-60 seconds of rest was provided.

3) Signal Acquisition: High-density sEMG signals were recorded from the forearm extensor muscles of the dominant arm with four disposal adhesive grids of 64 equally spaced electrodes (13 × 5 columns; 1 mm diameter; 4 mm inter-electrode distance; ELSCH064NM4, OT Bioelettronica, Italy). Before electrode application, the skin was shaved and then cleaned with alcohol. The sEMG signals were recorded in monopolar mode, bandpass filtered (10-900 Hz), and digitized at a sampling rate of 2048 Hz using a multichannel acquisition system (EMG-Quattrocento; 400-channel EMG amplifier, OT Bioelettronica, Italy). For more detail please refer to our previous work [29]. The grasping force was measured with a customized s-shape transducer and sampled at 10000 Hz.

D. Signal Processing

The raw high-density sEMG signals were digitally band-pass filtered (20 - 500 Hz, fourth-order Butterworth) before decomposed offline with normal (CKC and fastICA) and enhanced decomposition method. CKC and fastICA allowed a highly reliable identification of motor unit firing patterns over a broad range of voluntary contractions. For the simulated signals, all decomposed pulses were compared to the ground truth (simulated firings). Only pulses with a rate of agreement (RoA [30], [31]) greater than 0.3 were kept for further analysis. Sensitivity and precision were also used to evaluate the decomposition accuracy:

$$RoA_j = \frac{C_j}{A_j + B_j - C_j}$$
$$Sensitivity = \frac{TP}{TP + FN}$$
$$Precision = \frac{TP}{TP + FP} \tag{4}$$

where C_j denotes the number of discharges correctly identified for the jth motor unit, A_j and B_j are the numbers of discharges from decomposition and simulation (ground truth). The TP (true positive), FN (false negative) and FP (false positive) indicate the number of correctly identified discharges, the number of non-identified discharges, and the number of misidentified discharges, respectively.

For the experimental signal, only pulses with pulse-to-noise ratio (PNR [17]) greater than 25dB, silhouette (SIL [3]) greater than 0.8, coefficient of variation (CoV [32], [33]) below 40% and spike count (SC) greater than 5Hz were selected for further analysis. Motor unit action potentials were extracted via spike-triggered averaging (STA) the high-density sEMG in 30ms windows, centered at the spike instants [34], [35], [36]. It is worth noting that only the fastICA algorithm was used for the experimental signals because, in our case, fastICA decoded a greater number of motor units compared to CKC:

$$PNR_j = 10 \cdot log(\frac{E(\hat{s_j}(n) \mid_{\hat{s_j}(n) \geq r})}{E(\hat{s_j}(n) \mid_{\hat{s_j}(n) < r})}) \tag{5}$$

where $E(x \mid_{\hat{s_j}(n) \geq r})$ and $E(x \mid_{\hat{s_j}(n) < r})$ denote the mean across all time moments in which the jth motor unit is estimated to have or not have discharged, respectively.

During the enhanced decomposition that we proposed, one key point is to avoid duplicates. For example, in a simulated trial of 50% excitation level, a total of 100 motor units were activated, but the normal algorithm only managed to decode 38 of them. To acquire as many reliable motor units as possible, we proceeded with the enhanced decomposition procedure. We gathered all the MU filters (155 in total) that were successfully decoded during lower excitation levels (i.e., 32 at 10%, 43 at 20%, 39 at 30%, and 41 at 40%) and set them as the initialization vectors for the algorithm to converge. The resulting pulses were first compared to each other, and one of each pair with RoA > 0.3 was discarded because it is very likely that one motor unit was activated and decoded in several trials. We then compared the resulting pulses to the ground truth, focusing on the part that the normal decomposition failed to decode. If RoA > 0.3, it was considered successfully decoded. For the experimental signals, pulses were considered successfully decoded if they satisfied the filtering criteria mentioned earlier and had a RoA less than 0.3 compared to those decomposed using normal methods.

We also calculated the correlation between the normalized force signal and CST. As force increases, if the number of motor units decreases significantly due to heavy superimposition, the level of neural excitation no longer correlates directly with force level. This can impact the accuracy of CST-based force estimation tasks during varying force levels.

E. Statistical Analysis

Statistical analyses were performed using IBM SPSS Statistics v26 for Windows (SPSS Statistics, IBM Corporation). The Shapiro-Wilk test was used to assess the normality of the distribution of data. All the variables in the analysis did not deviate from a normal distribution. A repeated-measure ANOVA was performed to determine if the mean decomposed number of motor units differed between different trials. In order to estimate the strength of neural drive between different muscle areas, we used one-way ANOVA to compare the mean decomposed motor unit number from different electrode grids. Data were reported as means and S.D. Significance was accepted for P-values less than 0.05.

III. RESULT

The results in Table I present the average number of decomposed motor units for the simulated signal across six motor pools. All motor units were (RoA > 0.3, Rate of Agreement) matched to the ground-truth firing trains. The results were reported for four different SNRs and across seven excitation levels. Most importantly, the comparison between the number of motor units before and after enhanced decoding was conducted for both CKC and fastICA algorithms. The number increase rate for each SNR level was calculated and presented in Figure 2. we achieved an average increase rate of 135.4% ± 62.5% and 63.6% ± 20.2% for CKC and fastICA, respectively. There was no significant difference between different SNRs. The bar chart in Figure 2 also illustrates individual examples comparing the number of motor units decoded before and after enhancement. The comparisons are made at different force levels. No change is observed at the 10% excitation level, as it represents the lowest force level.

We also compared the sensitivity (SE) and precision (PR) before and after enhanced decomposition in Figure 3. As the force level increases, due to the effect of superimposition, both sensitivity and precision show an overall decreasing trend if MU filters were directly reused. However, the sensitivity and precision of motor units acquired from the enhanced procedure did not exhibit a significant drop. This result supports our hypothesis that during the reuse of MU filters, the algorithm undergoes a certain adaptive process, leading to accurate results. The adaptive process of MU filters to new signals is illustrated with a representative example in Figure 4. After being introduced as the initialization vector to the algorithm, the MU filter undergoes a series of iterations. It is assumed that with varying levels of superimposition, the MU filters might
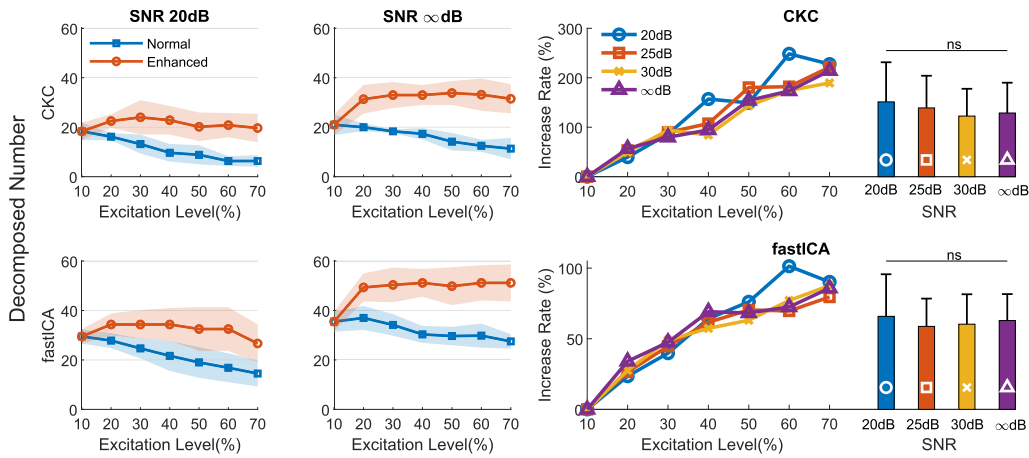
Fig. 2. Number of motor units decomposed and the increase rate over distinct excitation levels throughout multiple SNRs from simulated signals. The results were demonstrated as average (solid line) and standard deviation (shaded area). The x-axis denotes excitation levels, and the y-axis represents the number of motor units decomposed using the CKC and fastICA algorithms at 20 dB and ∞ dB SNR. The increase rate (right column) denoted the ratio of increase in the number of motor units after enhanced decoding. It increased along excitation levels and was compared across 4 SNRs in the bar plot. There was no significant difference in the increase rate across different noise levels (P > 0.05).

TABLE I
DECOMPOSED NUMBER OF MOTOR UNITS FROM
SIX SEPARATE DATABASES

SNR	Level	CKC		fastICA	
		Normal	Enhanced	Normal	Enhanced
20 dB	10%	18.3±3.5	-	29.5±2.8	-
	20%	16.2±1.5	22.5±2.7	27.8±3.0	34.3±4.5
	30%	13.1±3.8	24.0±6.9	24.6±4.0	34.3±5.8
	40%	9.6±3.5	22.8±5.7	21.6±6.0	34.3±6.6
	50%	8.8±3.8	20.1±5.7	19.0±6.2	32.5±8.8
	60%	6.3±1.9	20.8±4.9	16.8±5.8	32.5±8.8
	70%	6.3±2.3	19.6±5.7	14.5±5.2	26.6±7.7
25 dB	10%	20.0±3.4	-	31.5±1.9	-
	20%	18.6±2.1	28.6±6.6	32.1±1.6	40.6±3.6
	30%	15.0±3.6	27.8±4.0	27.5±3.0	39.6±5.6
	40%	14.0±3.5	28.1±6.2	27.0±5.2	43.5±8.6
	50%	10.5±3.2	28.0±6.6	24.0±6.8	40.3±10.0
	60%	9.6±3.0	25.5±7.0	24.0±6.0	40.3±9.1
	70%	9.0±3.6	25.6±5.2	21.5±4.1	38.6±9.2
30 dB	10%	20.3±1.6	-	32.3±2.2	-
	20%	18.5±1.6	27.5±1.5	33.0±3.5	42.0±4.4
	30%	15.1±3.1	28.8±2.9	30.1±4.7	45.0±7.7
	40%	15.6±1.5	28.8±2.9	28.8±3.1	45.3±5.1
	50%	12.3±3.5	28.6±4.9	27.3±4.6	44.1±7.1
	60%	10.8±3.4	28.1±6.9	25.1±4.8	44.3±7.8
	70%	10.0±3.4	26.6±5.9	23.6±7.1	42.8±9.5
∞ dB	10%	21.0±4.1	-	35.3±4.0	-
	20%	20.0±1.5	31.3±5.8	37.0±4.8	49.3±5.6
	30%	18.3±0.8	33.0±5.2	34.1±4.3	50.3±7.0
	40%	17.3±2.3	33.0±4.0	30.3±3.4	51.1±5.6
	50%	14.1±3.5	33.8±4.8	29.6±3.7	49.8±7.6
	60%	12.5±2.4	33.1±6.5	29.8±4.8	51.1±7.1
	70%	11.3±4.3	31.5±5.8	27.5±2.9	51.1±7.4

have changed slightly. Sensitivity, precision, and RoA were monitored during these iterations. Significant improvements in SE, Pr, and RoA were observed compared to directly reusing the MU filters. We also compared the maximum and minimum PP amplitudes of MUAPs before and after enhanced decoding, as shown in Figure 5. The results indicated that the minimum PP amplitudes were significantly lower for the enhanced decoding (P < 0.05), while there was no statistical difference between the maximum PP amplitudes for both methods.

For the experimental signal, the detailed number of decomposed motor units is presented in Table II. This number represents the total number of motor units decoded across the four electrode grids. Individual examples were illustrated in Figure 6, along with the overall increase rate observed after the enhanced process for all subjects during varying force contractions. Our method managed to decode 21.8% ± 10.9% more motor units for all the subjects. The increase rates for each subject were: 16.3%, 15.5%, 8.1%, 16.9%, 26.7%, 42.9%, 17.8%, 29.8%. It is evident that as the force level increases, the increase ratio also rises. The increase rates for the 70% and 90% levels were significantly higher than that of the 30% level.

Two sets of motor units were characterized by their action potentials and discharge rates, each of which was decoded from the same initial MU filter (Figure 7). Motor units activated during 30 % MVC can be tracked at higher force levels, ranging from 50 % to 90 %. There was a slight increase in discharge rates as force developed. The simulation in Figure 8 indicated the normally decoded motor units (blue ones) tend to have higher recruitment thresholds, and the number of blue motor units decreases with increasing force contractions. After enhanced decoding, the total number of decoded motor units increases with force contractions. The lower figure indicated that blue motor units tend to have larger sizes and bigger PP values compared to the orange ones.

The correlation between force and CST is shown in Figure 9 with two individual examples. The lower part of the figure demonstrates how our method improves the correlation across subjects without any additional training. After fully exploring the decoded number of motor units, the force-CST correlation increased by 64.6%, from 0.41 to 0.64, averaged across all subjects.

IV. DISCUSSION

A. Unveiling the Characteristics of Overlooked Motor Units

The total number of motor units in different muscles in the human body generally ranges from a few hundred [15] (e.g., 119 in the First Dorsal Interossei to 774 in the Biceps
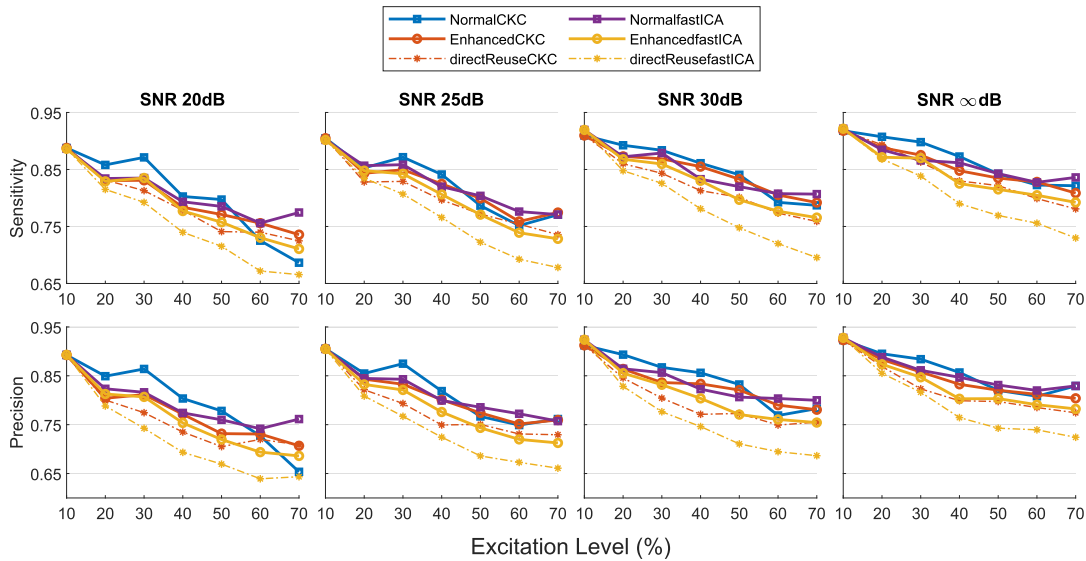
Fig. 3. Sensitivity and precision of motor units decoded from normal and enhanced procedures. The results were presented across four SNR levels with averages (solid lines) and standard deviations (shaded areas). The sensitivity and precision showed no significant differences between normal and enhanced results for both CKC and fastICA methods ($P > 0.05$). The sensitivity and precision when directly reusing the MU filters (directReuse) dropped significantly compared to the enhanced method ($P < 0.05$).

TABLE II
DECOMPOSED NUMBER OF MOTOR UNITS FROM EIGHT SUBJECTS

Subjects	#1		#2		#3		#4	
	Normal	Enhanced	Normal	Enhanced	Normal	Enhanced	Normal	Enhanced
10%	1.7±0.5	-	7.7±2.9	-	22.7±3.7	-	20.7±1.7	-
30%	6.0±0.0	6.5±0.5	22.7±1.2	23.2±2.0	29.5±2.5	30.7±3.3	21.5±2.6	23.2±3.3
50%	10.3±0.5	11.2±0.9	28.0±4.6	31.7±4.3	28.7±3.1	31.2±1.8	24.7±3.1	28.0±1.8
70%	6.0±0.8	7.3±1.5	17.2±4.1	21.0±6.0	36.7±2.5	41.0±2.9	30.2±5.5	35.7±4.5
90%	8.7±0.5	11.0±1.6	21.7±5.3	27.2±6.1	40.7±3.0	44.2±5.1	31.7±4.8	39.5±6.0

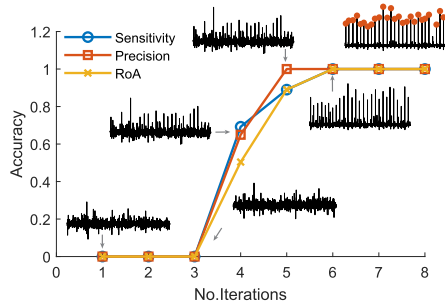| Subjects	#5		#6		#7		#8	
	Normal	Enhanced	Normal	Enhanced	Normal	Enhanced	Normal	Enhanced
10%	4.7±2.2	-	11.5±1.7	-	3.7±2.7	-	4.5±1.0	-
30%	7.5±2.6	8.2±1.9	7.7±0.9	8.5±1.2	8.2±0.9	8.5±1.2	4.5±1.7	5.2±1.7
50%	7.5±2.0	9.5±3.1	9.8±2.0	10.2±2.0	10.2±1.2	12.0±1.4	8.7±3.4	9.2±3.8
70%	11.2±1.2	13.0±0.8	8.0±0.8	11.7±2.8	12.0±3.4	15.7±4.1	2.7±1.2	4.7±2.9
90%	10.2±4.5	14.0±5.0	5.5±1.7	10.0±1.4	12.5±1.7	15.0±1.4	4.0±2.4	5.7±3.7

Fig. 4. Representative example of the automatic adaptation of MU filters to new signals. At each iteration, sensitivity, precision, and RoA improved, particularly between the 3rd and 5th iterations. Within a total of fewer than 8 iterations, we acquired the final firing patterns for the MU filters in the new signal using peak detection.
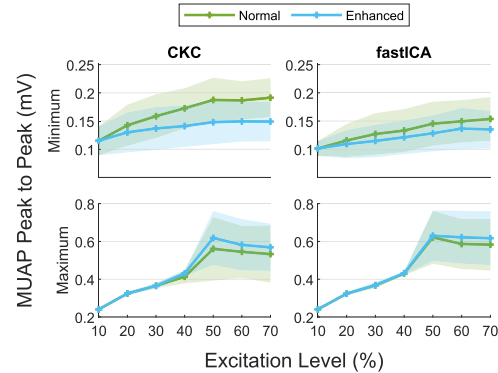

Fig. 5. Comparison of motor unit peak-to-peak (PP) amplitudes decomposed from normal and enhanced procedures across varying excitation levels. Two normal decomposition methods, CKC and fastICA, were compared. The minimum PP value represents the lower limit of a motor unit that the algorithm can decode, while the maximum PP value represents the upper limit. The results are presented as averages (solid lines) with standard deviations (shaded areas).

Brachii). Among these, the contraction of muscles is regulated by the number of activated motor units. When a motor unit is activated, its action potential can be detected by sEMG electrodes [37]. Therefore, to achieve a comprehensive understanding of muscle activation, it is crucial to decode as many

active motor units as possible from sEMG signals. Motor unit decomposition algorithms have consistently been a popular
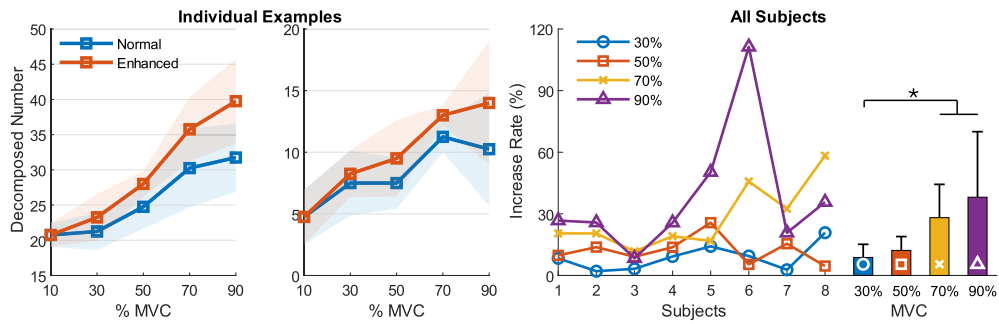
Fig. 6. Number of decomposed motor units and increase rate from the experimental signal of eight subjects. The results (left column) were demonstrated as average (solid line) and standard deviation (shaded area). We also compared the increase rate (right column) across four different force levels, representing the ratio of increase in the number of motor units after enhanced decoding. The symbol $*$ indicates $P < 0.05$.
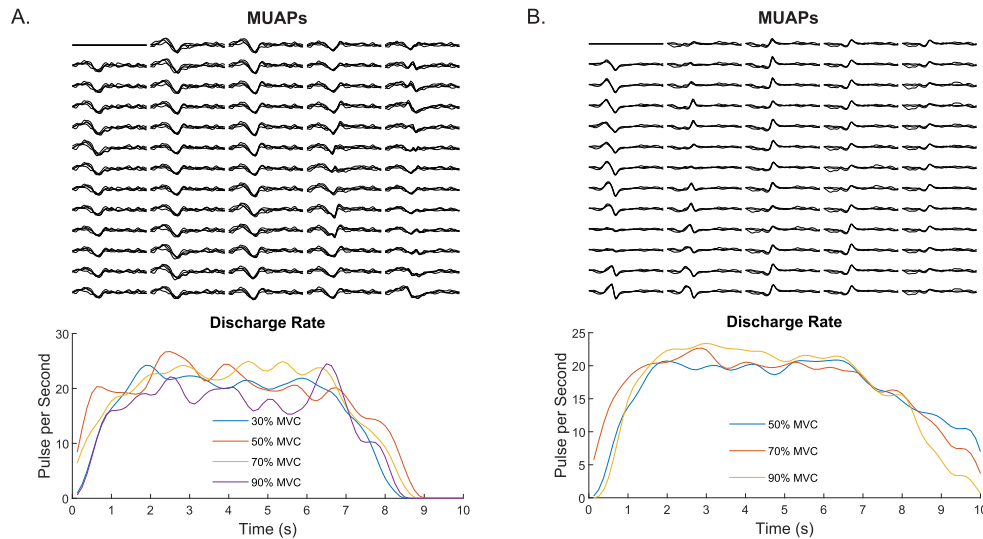

Fig. 7. Motor unit action potentials and firing properties across different force levels from experimental signals. A and B represent two motor unit sets that were successfully decoded from the same MU filter four and three times, respectively, across different excitation levels.
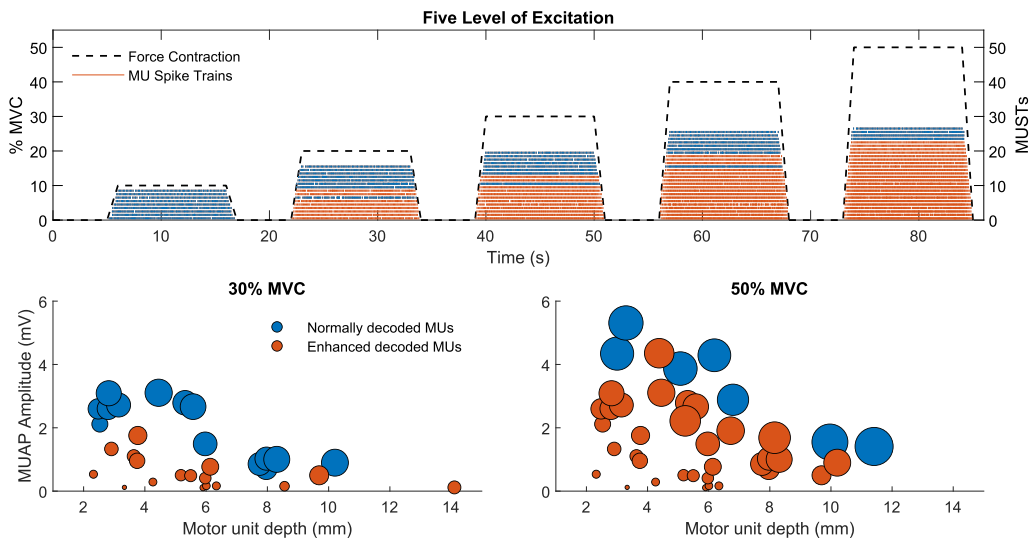

Fig. 8. The simulation results comparing motor units decoded before and after enhanced decoding. The colors blue and orange represent motor units decoded before and after enhanced decoding, respectively. The upper figure compares discharge patterns across five different force contractions, with each motor unit arranged based on its first discharge time. The lower figure compares the size, peak-to-peak (PP) amplitude, and motor unit depth at 30% and 50% force contractions. Each solid circle represents a motor unit, with the radius indicating its size. Large and superficial motor units exhibit a larger peak-to-peak amplitude.

topic in recent years. Compared to conventional methods, an increase in the number of decoded motor units serves as an important performance metric. Although decoding algorithms consistently contribute to an increase in the number of decoded
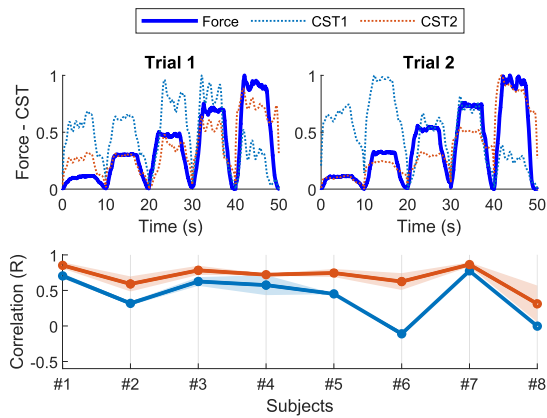
Fig. 9. The experimental force-to-CST curve and their correlation across all subjects. The upper figure shows two example trials of the neural response CST to the exerted force recordings (10% - 90%). CST1 and CST2 represent the cumulative spike trains before and after enhanced decoding, respectively. The rest phases between different force levels during the experiments were removed for simplicity. The lower figure illustrates the correlation between force and CST for all subjects calculated across all force levels. The correlation between CST2 and force was significantly higher than that of CST1 ($P < 0.001$).

motor units at specific force levels, these results are relatively discrete. In other words, varying force involves continuous activation of motor units across the entire motor pool, there is a notable lack of performance assessment for algorithms under continuous force variations. Consequently, when the exerted force continuously changes, the neural activity extracted from decoded motor units does not show a corresponding continuous response. In particular, when the exerted force increases substantially, a significant gap between force signal and neural activity is observed [22].

One possible reason for this phenomenon is the inability of current decoding algorithms to overcome severe superimposition as force increases. When force excitation increases, larger motor units with higher PP values are recruited (Figure 8). The amplitude of large motor units can be several to tens of times greater than that of smaller motor units. This causes current algorithms to mistakenly treat the activity of smaller motor units as noise. Without prior knowledge directing the algorithm to actively seek out these smaller motor units, decoding them becomes quite difficult. However, this assumption relies on the fact that these smaller motor units are indeed being activated. The widely recognized size principle provides a basis for this reuse, as it supports the idea that smaller motor units are recruited first and should be detectable if appropriately filtered.

B. Neural Responses to Varying Force Levels

The force generated by a muscle during voluntary contraction is determined by the recruitment of motor units and the rates at which they discharge action potentials, known as rate coding. The nervous system regulates muscle force by modulating both motor unit recruitment and rate coding over the muscle's operational range [37]. During neural interfacing, the current demand for decoding algorithms is to comprehensively address both motor unit recruitment and rate coding. In terms of rate coding, once the decoding algorithm has acquired the MU filter (or separation vector), real-time computation of

discharge rates becomes feasible. Most voluntary movements involve motor units firing action potentials between 10–30 pps, with discharge rates often adjusting by 5–10 pps during tasks like submaximal contractions. However, concerning motor unit recruitment, decoding algorithms encounter a challenge, as they cannot predict in advance how many MUs within the MU pool are activated and subsequently decoded. The lack of prior knowledge about the active motor unit quantity can significantly impact our understanding of the neural system's force control. Accurately predicting the number of activated motor units during varying force levels can be challenging, given that even the gold standard invasive electrode can only capture the activity of motor units at specific points. Although the estimation of motor unit numbers in this study is inherently an approximation, this approach brings meaningful improvements to the current findings.

C. Limitations

There are several limitations to this study. First, although reusing MU filters from low to high contraction levels has been proven efficient for multiple muscles, there are still some scenarios where motor unit recruitment does not follow a fixed order [38]. In such cases, our enhanced process might not be effective enough. Secondly, despite successfully identifying many active motor units, we still cannot decode all of the activated motor units in the muscle. On the one hand, sEMG has a limited pick-up volume [39], allowing us to detect only a small portion of the active motor units in the muscle using surface electrodes. On the other hand, heavy superimposition remains an issue, preventing precise decoding of all motor units. Thirdly, muscle force is determined by both motor unit recruitment and discharge modulation [27]. While our method improves force estimation from CST, its impact on force estimation accuracy is limited, as factors such as twitch response and other elements also play a significant role in force generation.

V. CONCLUSION

In summary, we introduced an adaptive method to enhance motor unit decomposition by manually adjusting the initialization direction of our algorithm. This approach successfully decoded a substantial number of reliable MUs by reutilizing MU filters in a novel manner. Our results demonstrated significant improvements in the number of decoded MUs and the correlation between force and cumulative spike trains. This method shows promise for accurately decoding MUs across varying force levels, enhancing the reliability of sEMG signal analysis.

REFERENCES

[1] A. Holobar and D. Farina, "Noninvasive neural interfacing with wearable muscle sensors: Combining convolutive blind source separation methods and deep learning techniques for neural decoding," *IEEE Signal Process. Mag.*, vol. 38, no. 4, pp. 103–118, Jul. 2021.

[2] C. J. De Luca, A. Adam, R. Wotiz, L. D. Gilmore, and S. H. Nawab, "Decomposition of surface EMG signals," *J. Neurophysiology*, vol. 96, no. 3, pp. 1646–1657, Sep. 2006.

[3] F. Negro, S. Muceli, A. M. Castronovo, A. Holobar, and D. Farina, "Multi-channel intramuscular and surface EMG decomposition by convolutive blind source separation," *J. Neural Eng.*, vol. 13, no. 2, Apr. 2016, Art. no. 026027.

[4] G. R. Naik, S. E. Selvan, M. Gobbo, A. Acharyya, and H. T. Nguyen, "Principal component analysis applied to surface electromyography: A comprehensive review," *IEEE Access*, vol. 4, pp. 4025–4037, 2016.

[5] V. Glaser and A. Holobar, "Motor unit identification from high-density surface electromyograms in repeated dynamic muscle contractions," *IEEE Trans. Neural Syst. Rehabil. Eng.*, vol. 27, no. 1, pp. 66–75, Jan. 2019.

[6] M. Chen and P. Zhou, "A novel framework based on FastICA for high density surface EMG decomposition," *IEEE Trans. Neural Syst. Rehabil. Eng.*, vol. 24, no. 1, pp. 117–127, Jan. 2016.

[7] Y. Xu, Y. Yu, M. Xia, X. Sheng, and X. Zhu, "A novel and efficient surface electromyography decomposition algorithm using local spatial information," *IEEE J. Biomed. Health Informat.*, vol. 27, no. 1, pp. 286–295, Jan. 2023.

[8] C. Chen, S. Ma, X. Sheng, and X. Zhu, "A peel-off convolution kernel compensation method for surface electromyography decomposition," *Biomed. Signal Process. Control*, vol. 85, Aug. 2023, Art. no. 104897.

[9] Y. Wen, S. Avrillon, J. C. Hernandez-Pavon, S. J. Kim, F. Hug, and J. L. Pons, "A convolutional neural network to identify motor units from high-density surface electromyography signals in real time," *J. Neural Eng.*, vol. 18, no. 5, Oct. 2021, Art. no. 056003.

[10] J. Škarabot et al., "Decoding firings of a large population of human motor units from high-density surface electromyogram in response to transcranial magnetic stimulation," *J. Physiol.*, vol. 601, no. 10, pp. 1719–1744, May 2023.

[11] M. Rácz et al., "Spike detection and sorting with deep learning," *J. Neural Eng.*, vol. 17, no. 1, Jan. 2020, Art. no. 016038.

[12] A. K. Clarke et al., "Deep learning for robust decomposition of high-density surface EMG signals," *IEEE Trans. Biomed. Eng.*, vol. 68, no. 2, pp. 526–534, Feb. 2021.

[13] A. Del Vecchio, A. Holobar, D. Falla, F. Felici, R. M. Enoka, and D. Farina, "Tutorial: Analysis of motor unit discharge characteristics from high-density surface EMG signals," *J. Electromyogr. Kinesiol.*, vol. 53, Aug. 2020, Art. no. 102426.

[14] A. D. Vecchio and D. Farina, "Interfacing the neural output of the spinal cord: Robust and reliable longitudinal identification of motor neurons in humans," *J. Neural Eng.*, vol. 17, no. 1, Feb. 2020, Art. no. 016003.

[15] B. Feinstein, B. Lindegård, E. Nyman, and G. Wohlfart, "Morphologic studies of motor units in normal human muscles," *Cells Tissues Organs*, vol. 23, no. 2, pp. 127–142, 1955.

[16] A. Francic and A. Holobar, "On the reuse of motor unit filters in high density surface electromyograms recorded at different contraction levels," *IEEE Access*, vol. 9, pp. 115227–115236, 2021.

[17] C. Chen, S. Ma, X. Sheng, D. Farina, and X. Zhu, "Adaptive real-time identification of motor unit discharges from non-stationary high-density surface electromyographic signals," *IEEE Trans. Biomed. Eng.*, vol. 67, no. 12, pp. 3501–3509, Dec. 2020.

[18] Y. Xu, Y. Yu, Z. Zhao, C. Chen, and X. Sheng, "Cumulative spike train estimation for muscle excitation assessment from surface EMG using spatial spike detection," *IEEE J. Biomed. Health Informat.*, vol. 27, no. 11, pp. 5335–5344, Nov. 2023.

[19] C. Chen, Y. Yu, X. Sheng, and X. Zhu, "Non-invasive analysis of motor unit activation during simultaneous and continuous wrist movements," *IEEE J. Biomed. Health Informat.*, vol. 26, no. 5, pp. 2106–2115, May 2022.

[20] Y. Xu, Y. Yu, Z. Zhao, and X. Sheng, "Decoding multi-DoF movements using a CST-based force generation model with single-DoF training," *IEEE Trans. Neural Syst. Rehabil. Eng.*, vol. 32, pp. 974–982, 2024.

[21] X. Hu, W. Z. Rymer, and N. L. Suresh, "Motor unit pool organization examined via spike-triggered averaging of the surface electromyogram," *J. Neurophysiol.*, vol. 110, no. 5, pp. 1205–1220, Sep. 2013.

[22] E. Martinez-Valdes et al., "Modulations in motor unit discharge are related to changes in fascicle length during isometric contractions," *J. Appl. Physiol.*, vol. 133, no. 5, pp. 1136–1148, Nov. 2022.

[23] X. Hu, W. Z. Rymer, and N. L. Suresh, "Control of motor unit firing during step-like increases in voluntary force," *Frontiers Human Neurosci.*, vol. 8, p. 721, Sep. 2014.

[24] A. Holobar and D. Zazula, "Multichannel blind source separation using convolution kernel compensation," *IEEE Trans. Signal Process.*, vol. 55, no. 9, pp. 4487–4496, Sep. 2007.

[25] A. Holobar and D. Zazula, "Gradient convolution kernel compensation applied to surface electromyograms," in *Independent Component Analysis and Signal Separation*. Berlin, Germany: Springer, 2007, pp. 617–624.

[26] E. Henneman, "Relation between size of neurons and their susceptibility to discharge," *Science*, vol. 126, no. 3287, pp. 1345–1347, Dec. 1957.

[27] A. J. Fuglevand, D. A. Winter, and A. E. Patla, "Models of recruitment and rate coding organization in motor-unit pools," *J. Neurophysiol.*, vol. 70, no. 6, pp. 2470–2488, Dec. 1993.

[28] D. Farina, L. Mesin, S. Martina, and R. Merletti, "A surface EMG generation model with multilayer cylindrical description of the volume conductor," *IEEE Trans. Biomed. Eng.*, vol. 51, no. 3, pp. 415–426, Mar. 2004.

[29] M. Xia, C. Chen, Y. Xu, Y. Li, X. Sheng, and H. Ding, "Extracting individual muscle drive and activity from high-density surface electromyography signals based on the center of gravity of motor unit," *IEEE Trans. Biomed. Eng.*, vol. 70, no. 10, pp. 2852–2862, Oct. 2023.

[30] A. Holobar, M. A. Minetto, A. Botter, and D. Farina, "Identification of motor unit discharge patterns from high-density surface EMG during high contraction levels," in *Proc. IFMBE*. Berlin, Germany: Springer, 2011, pp. 1165–1168.

[31] C. Chen, S. Ma, Y. Yu, X. Sheng, and X. Zhu, "Segment-wise decomposition of surface electromyography to identify discharges across motor neuron populations," *IEEE Trans. Neural Syst. Rehabil. Eng.*, vol. 30, pp. 2012–2021, 2022.

[32] C. M. Germer, D. Farina, L. A. Elias, S. Nuccio, F. Hug, and A. Del Vecchio, "Surface EMG cross talk quantified at the motor unit population level for muscles of the hand, thigh, and calf," *J. Appl. Physiol.*, vol. 131, no. 2, pp. 808–820, Aug. 2021.

[33] A. Holobar, M. A. Minetto, A. Botter, F. Negro, and D. Farina, "Experimental analysis of accuracy in the identification of motor unit spike trains from high-density surface EMG," *IEEE Trans. Neural Syst. Rehabil. Eng.*, vol. 18, no. 3, pp. 221–229, Jun. 2010.

[34] D. Farina, L. Arendt-Nielsen, R. Merletti, and T. Graven-Nielsen, "Assessment of single motor unit conduction velocity during sustained contractions of the tibialis anterior muscle with advanced spike triggered averaging," *J. Neurosci. Methods*, vol. 115, no. 1, pp. 1–12, Mar. 2002.

[35] D. Farina, A. Holobar, R. Merletti, and R. M. Enoka, "Decoding the neural drive to muscles from the surface electromyogram," *Clin. Neurophysiol.*, vol. 121, no. 10, pp. 1616–1623, Oct. 2010.

[36] A. Malanda, J. Navallas, J. Rodriguez-Falces, I. Rodriguez-Carreño, and L. Gila, "Averaging methods for extracting representative waveforms from motor unit action potential trains," *J. Electromyogr. Kinesiol.*, vol. 25, no. 4, pp. 581–595, Aug. 2015.

[37] P. A. Lynn, N. D. Bettles, A. D. Hughes, and S. W. Johnson, "Influence of electrode geometry on bipolar recordings of the surface electromyogram," *Med. Biol. Eng. Comput.*, vol. 16, no. 6, pp. 651–660, Nov. 1978.

[38] F. Hug, S. Avrillon, J. Ibáñez, and D. Farina, "Common synaptic input, synergies and size principle: Control of spinal motor neurons for movement generation," *J. Physiol.*, vol. 601, no. 1, pp. 11–20, Jan. 2023.

[39] T. M. Vieira, A. Botter, S. Muceli, and D. Farina, "Specificity of surface EMG recordings for gastrocnemius during upright standing," *Sci. Rep.*, vol. 7, no. 1, p. 13300, Oct. 2017.